Rheol Acta 35:531–544 (1996)

ORIGINAL CONTRIBUTION

Georgios C. Georgiou

Extrusion of a compressible Newtonian fluid with periodic inflow and slip at the wall

Received: 24 May 1996
Accepted: 26 August 1996

Dedicated to the memory
of Prof. Tasos Papanastasiou

Dr. G.C. Georgiou (✉)
Department of Mathematics and Statistics
University of Cyprus
Kallipoleos 75
P.O. Box 537
1678 Nicosia, Cyprus

Abstract We explore a mechanism of extrusion instability, based on the combination of nonlinear slip and compressibility. We consider the time-dependent compressible Newtonian extrudate swell problem with slip at the wall. Steady-state solutions are unstable in regimes where the shear stress is a decreasing function of the velocity at the wall. Compressibility provides the means for the alternate storage and release of elastic energy, and, consequently, gives rise to periodic solutions. The added novelty in the present work is the assumption of periodic volumetric flow rate at the inlet of the die. This leads to more involved periodic responses and to free surface oscillations similar to those observed experimentally with the stick-slip instability. To numerically simulate the flow, we use finite elements in space and a fully-implicit scheme in time.

Key words Extrudate swell – compressible Newtonian flow – slip – time-dependent flow

Introduction

Flow instabilities occurring during the extrusion of polymeric fluids from capillaries and slits were first reported in the early 1960s. Since then, they have received considerable attention, because they have an adverse effect on the quality of the extrudate and thus limit the production rates. A whole range of surface defects has been observed above a critical value of the volumetric flow rate, the size and severity of which depend on the type of the polymer and the material of construction of the capillary. Comprehensive reviews on this subject can be found in Piau et al. (1990), Denn (1992) and Larson (1992). The different instability regimes are often studied in connection with the flow curve, i.e., the log-log plot of the pressure drop versus the flow rate (or, equivalently, the log-log plot of the wall shear stress versus the apparent shear rate).

The sequence of extrudate defects and the shape of the flow curve are not the same for all polymers. The experimental data of Kalika and Denn (1987) for a LLDPE, Hatzikiriakos and Dealy (1992a, b) for a HDPE, and Piau et al. (1990) for a linear polydimethylsiloxane, show that, for most linear polymers, the stable regime is followed by three distinct instability regimes, corresponding to the *sharkskin*, the *stick-slip* and the *gross fracture* instabilities. The flow curve consists of two positive-slope branches separated by an oscillatory part. The left branch corresponds to the stable and sharkskin regimes. In the latter, the extrudate surface is characterized by a small-scale, short-wavelength roughness. In many cases, a change of slope of the flow curve has been observed at the visual onset of sharkskin (Hill et al., 1990; Denn, 1992; Hatzikiriakos and Dealy, 1992a, b). To the oscillatory part of the flow curve, there corresponds the stick-slip instability. The pressure and the flow rate are periodic and the extrudate surface consists of alternating relatively smooth and sharkskin regions. Finally, the gross fracture regime, in which the surface of the extrudate is extremely irregular, corresponds to the right positive-slope branch of the flow curve.

A debate still exists as far as the origins and the mechanisms of extrusion instabilities are concerned. In

Rheologica Acta, Vol. 35, No. 6 (1996)

the stick-slip and gross melt fracture regimes, the flow from the die-entry region to the extrudate is time dependent (Larson, 1992). Piau and his co-workers argue that the flow instabilities in the gross melt fracture regime originate in the contraction region, where symmetry is lost and the flow destabilizes at high volumeric flow rates (Piau et al., 1990; Piau and El Kissi, 1992); they provide pictures showing the two upstream vortices oscillating in a knitting fashion, and suggest that the instability is convected to the extrudate through the die. Others, however, believe that the instabilities appear within the die and are most easily observed in extrusion through a long die (Denn, 1990, 1992). For the sharkskin defect, however, it is generally believed that it is initiated at or near the die exit (Moynihan et al., 1990). Indeed, some recent explanations proposed for sharkskin are based on the high stresses developed in the die exist region. Tremblay (1991) and El Kissi and Piau (1994) believe that sharkskin is a result of cracking of the fluid due to the formation, growth and coalescence of voids close to the die lip. Another explanation is provided by Chen and Joseph (1992) who assume that polymer segregation occurs near the exit and show that this can lead, under certain conditions, to short-wave instabilities.

Slip at the wall and constitutive instabilities are the most common explanations proposed for the stick-slip and gross fracture instabilities. These can be combined with other factors like melt compressibility, the pressure dependence of other material parameters and viscous heating (Denn, 1990; Larson, 1992). The importance of the role of slip in the stick-slip and gross fracture instabilities has gained ground in the last 10 years (Pearson, 1985; Denn, 1992; Larson, 1992). Some researchers suggest that slip triggers the sharkskin instability as well, and causes the change of slope of the flow curve at the visual onset of sharkskin (Hill et al., 1990; Denn, 1992; Hatzikiriakos and Dealy, 1992a, b). Slip might even be used to suppress extrudate distortions, as shown by Piau et al. (1995) who have eliminated cracks and surface distortions using slippery surfaces for the extrusion of polyethylenes.

Slip equations relate the slip velocity to the shear stress at the wall, the temperature, the pressure and material parameters. In most isothermal experimental data, the shear stress is a power of the slip velocity (Hatzikiriakos and Dealy, 1992b; Denn, 1992). More interesting are nonlinear slip equations similar to those proposed by El Kissi and Piau (1989) and Leonov (1990), i.e. slip equations with maxima and minima, meaning that the slip velocity is multi-valued over a certain range of the wall shear stress. The corresponding flow curves for Poiseuille flow exhibit maxima and minima too. To the above two empirical equations, we can also add the experimental data of Hatzikiriakos and Dealy (1992b) in which the slip velocity is multi-valued. Hatzikiriakos and Dealy (1992b) propose a power-law slip equation for each one of the two positive-slope branches of their experimental flow curve.

The linear stability analysis of the incompressible Newtonian Poiseuille flow with slip along the wall shows that steady-state solutions in the negative-slope regime of the slip equation are unstable to two-dimensional disturbances (Pearson and Petrie, 1965). Pearson (1985) suggested that, if bulk compressibility is taken into account, one would expect a periodic solution with self-sustained pressure and flow-rate oscillations similar to those observed in the stick-slip instability regime. This idea has been confirmed in a previous work (Georgiou and Crochet, 1994a), where the time-dependent compressible Newtonian Poiseuille flow with slip along the wall was solved numerically. Even though compressibility does not considerably alter the steady-state solutions, it has a dramatic effect on the flow dynamics. We have examined the dynamic response of the flow system to small perturbations of the steady-state solutions while keeping the volumetric flow rate at the inlet fixed, and shown that periodic solutions are eventually reached, in the negative slope regime of the flow curve. We have also solved the time-dependent compressible Newtonian extrudate-swell problem (Georgiou and Crochet, 1994b) showing that the pressure-drop and mass-flow-rate oscillations in the die generate waves on the surface of the extrudate, the amplitude and wavelength of which increase with compressibility.

The objective of the present work is to further explore the above mechanism of instability by assuming that the volumetric flow rate at the inlet of the die is periodic instead of constant. This assumption is more realistic since the volumetric flow rate is fixed only at the plane of the piston which moves with constant speed, that is, in the reservoir and not in the die. Moreover, it allows us to consider only the last section of the die without having to deal with whether the instabilities originate upstream in the die or even farther in the contraction region, as suggested by Piau and El Kissi (1992). Note, however, that including the reservoir region in the simulations would lead to more conclusive results for the role of compressibility, but this is beyond the scope of the current work.

We should also add that other simulations of extrusion instability proposed in the literature are based a) on the multi-valuedness of the constitutive equation (see, for example, Kolkka et al. (1988) and the review paper of Larson (1992), and b) on the combination of nonlinear slip and viscoelasticity. The latter mechanism does not require any multi-valuedness of the constitutive equation and is discussed elsewhere (Brasseur et al., 1996; Georgiou, 1996).

The governing equations and the boundary conditions for the time-dependent compressible Newtonian extrudate-swell problem are presented in the second section. In the third section, we give a brief description of the finite element formulation. A fully-implicit scheme is used for the time integration. Numerical results for both the Poiseuille and the extrudate-swell flows are presented and

discussed in the fourth section. Finally, our conclusions are summarized in the fifth section.

Governing equations

We consider the time-dependent, compressible, Newtonian extrudate-swell problem (Fig. 1). Subsequently, we shall be using the dimensionless forms of the equations. We scale the lengths by the radius of the tube R, the velocity $\boldsymbol{v}$ by a characteristic velocity V, and the pressure p and the components of the stress tensor $\boldsymbol{\sigma}$ by $\eta V/R$, where η is the viscosity (assumed to be independent of pressure). Moreover, the density ρ is scaled by the density ρ_0 at the reference pressure p_0, and the time by R/V. The continuity and the momentum equations for time-dependent compressible flow in the absence of body forces are as follows:

$$\frac{\partial \rho}{\partial t} + \nabla \cdot \rho \boldsymbol{v} = 0 \ , \tag{1}$$

$$\mathrm{Re}\,\rho \left(\frac{\partial \boldsymbol{v}}{\partial t} + \boldsymbol{v} \cdot \nabla \boldsymbol{v} \right) = \nabla \cdot \boldsymbol{\sigma} \ , \tag{2}$$

where Re is the Reynolds number defined as

$$\mathrm{Re} \equiv \frac{\rho_0 V R}{\eta} \ . \tag{3}$$

If the bulk viscosity is neglected, the dimensionless stress tensor for a compressible Newtonian fluid is given by

$$\boldsymbol{\sigma} = -p\boldsymbol{I} + [(\nabla \boldsymbol{v}) + (\nabla \boldsymbol{v})^T] - \frac{2}{3}\boldsymbol{I} \nabla \cdot \boldsymbol{v} \ , \tag{4}$$

where $\boldsymbol{I}$ is the unit tensor, and the superscript T denotes the transpose.

To express the density as a function of pressure, we use the linear expression

$$\rho = 1 + B(p - p_0) \ . \tag{5}$$

B is a dimensionless compressibility number defined as

$$B \equiv \frac{\beta \eta V}{R} \ , \tag{6}$$

where $\beta = -\frac{1}{V_0}\left(\frac{\partial V}{\partial p}\right)_{p_0, T}$ is the isothermal compressibility, which is assumed to be constant, and V_0 is the specific volume at the reference pressure p_0 and temperature T.

The boundary conditions are shown in Fig. 1. Along the wall of the die, the radial velocity component vanishes and slip is assumed to occur following the slip equation used by Georgiou and Crochet (1994a):

$$\sigma_w = A_1 \left(1 + \frac{A_2}{1 + A_3 v_w^2} \right) v_w \ , \tag{7}$$

where σ_w is the shear stress exerted by the fluid on the wall, v_w is the relative velocity of the fluid with respect to the wall, and A_1, A_2 and A_3 are dimensionless numbers resulting from the three material parameters of the slip equation (Georgiou and Crochet, 1994a). When A_2 is larger than 8, σ_w is a decreasing function in v_w over some intermediate range of v_w.

Along the axis of symmetry we have the usual symmetry conditions. The end of the jet is stress free. On the free surface of the extrudate, we impose vanishing normal and tangential stresses, i.e. we neglect surface tension:

$$\boldsymbol{n} \cdot \boldsymbol{\sigma} = \boldsymbol{0} \ , \tag{8}$$

where $\boldsymbol{n}$ is the outward unit vector normal to the free surface. If $h(z, t)$ is the unknown position of the free surface, then the kinematic condition is written as follows:

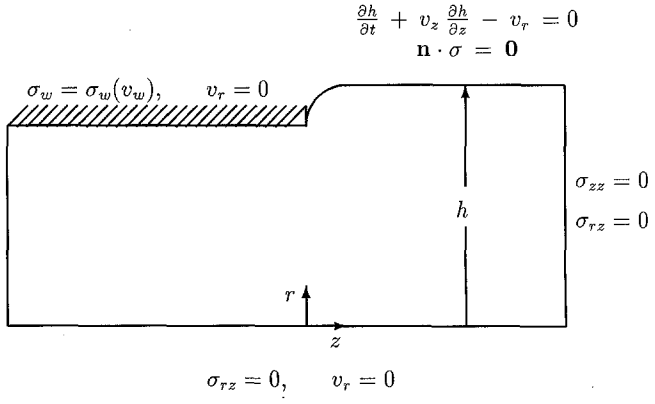

Fig. 1 Boundary conditions for the time-dependent compressible extrudate-swell problem with periodic inflow and slip at the wall

Rheologica Acta, Vol. 35, No. 6 (1996)

$$\frac{\partial h}{\partial t}+v_z\frac{\partial h}{\partial z}-v_r=0\ . \tag{9}$$

Eq. (9) is the additional equation needed for the calculation of $h(z,t)$.

At the inlet plane, we assume that the density is uniform and that the axial velocity is a parabolic function of r. These assumptions are obviously true for the incompressible Poiseuille flow. They are also consistent with the analytical solution for compressible Poiseuille flow when inertia is neglected and the velocity gradients across the die are much greater than in the direction of the flow (Georgiou and Crochet, 1994a). We easily obtain the following expression for v_z:

$$v_z=(2r^2-1)\,v_w^I+2(1-r^2)\,Q\ , \tag{10}$$

where v_w^I is the slip velocity at the inlet, and Q is the imposed volumetric flow rate. The slip velocity v_w^I is determined by invoking the slip Eq. (7):

$$4\,(v_w^I-Q)=-A_1\left[1+\frac{A_2}{1+A_3\,(v_w^I)^2}\right]v_w^I\ . \tag{11}$$

The value of v_w^I is unique provided that $A_2<8+32/A_1$, which implies that the volumetric flow rate is a monotonically increasing function of v_w^I.

Finally, in the time-dependent case, we assume that either the volumetric flow rate at the inlet is fixed or it varies sinusoidally with time:

$$Q=Q_0+\Delta Q\sin\omega t\ , \tag{12}$$

where Q_0 is the volumetric flow rate at $t=0$, ΔQ is the amplitude and ω is the angular velocity.

Numerical method

We use the finite element method for solving the extrudate-swell problem. The unknown position of the free surface is calculated together with the velocity and pressure fields, i.e., we use the full-Newton iteration method (Georgiou et al., 1988). The density is eliminated by means of the equation of state (5). We use the standard biquadratic-velocity (P^2-C^0) and bilinear-pressure (P^1-C^0) elements with a quadratic representation for the position h of the free surface. Let Ψ^j, Φ^j and χ^j denote the bilinear, biquadratic and quadratic shape functions, respectively. The unknowns p, v, and h are expanded as follows:

$$p=\sum_j^{N_p}p^j\,\Psi^j\ ;\quad v=\sum_j^{N_v}v^j\,\Phi^j\ ;\quad h=\sum_j^{N_h}h^j\,\chi^j\ . \tag{13}$$

Here, p^j, v^j and h^j are the values of the unknowns at the jth node, and N_p, N_v and N_h are the numbers of pressure, velocity, and free-surface nodes, respectively.

For the spatial discretization of the problem, we use the Galerkin forms of the continuity, momentum and kinematic equations. For steady flow, the discretized Galerkin equations read:

$$\int_\Omega \nabla\cdot[(1+Bp)\,v]\,\Psi^i\,d\Omega=0\ ,\quad i=1,2,\ldots,N_p\ , \tag{14}$$

$$\int_\Omega [\mathrm{Re}(1+Bp)\,v\cdot\nabla v\,\Phi^i+\sigma\cdot\nabla\Phi^i]\,d\Omega-\int_{\partial\Omega}n\cdot\sigma\,\Phi^i\,ds=0,\quad i=1,2,\ldots,N_v\ , \tag{15}$$

$$\int_{\text{Free surface}}\left(v_z\frac{\partial h}{\partial z}-v_r\right)\chi^i\,ds=0\ ,\quad i=1,2,\ldots,N_h\ , \tag{16}$$

where Ω and $\partial\Omega$ denote the domain and its boundary, respectively. We use the Newton-Raphson method and a frontal solver in order to solve the nonlinear system of Eqs. (14)–(16).

In applying the boundary conditions, we note that only the contribution to the z-momentum due to the slip along the wall,

$$-\int_{\text{Wall}}\sigma_w\,\Phi^i\,ds=-\int_{\text{Wall}}A_1\left(1+\frac{A_2}{1+A_3\,v_w^2}\right)v_w\,\Phi^i\,r\,dr\ , \tag{17}$$

is calculated in the boundary integral of Eq. (15). The discretized z-momentum equations along the inlet are replaced by

$$\int_{\text{Inlet}}[v_z-(2r^2-1)\,v_w^I-2(1-r^2)\,Q(t)]\Phi^i\,r\,dr=0\ . \tag{18}$$

For time-dependent flow, we use the standard fully-implicit (Euler backward-difference) scheme. As an example, the Galerkin form of momentum equations at time t^{n+1} becomes:

$$\int_\Omega\left[\mathrm{Re}(1+Bp^n)\left(\frac{v^{n+1}-v^n}{\Delta t}+v^{n+1}\cdot\nabla v^{n+1}\right)\Phi^i+\sigma^{n+1}\cdot\nabla\Phi^i\right]d\Omega-\int_{\partial\Omega}n\cdot\sigma^{n+1}\,\Phi^i\,ds=0\ ,\quad i=1,2,\ldots,N_v\ , \tag{19}$$

where Δt is the time step and (p^n,v^n,h^n) is the solution at time t^n. The residuals of the continuity and kinematic equations involve time derivatives as well, and they are modified in a similar manner. Attention is required when calculating the time derivatives in the extrudate region

because the nodes move following the motion of the free surface. If x^n and v_{mesh} are the position and the velocity of a node at time t^n, then the time derivative of v_z at the new nodal position x^{n+1} at time t^{n+1} is given by

$$\frac{\partial v_z^{n+1}(x^{n+1})}{\partial t} = \frac{v_z^{n+1}(x^{n+1}) - v_z^n(x^n)}{\Delta t} - v_{mesh} \cdot \nabla v_z^n(x^n) \quad (20)$$

Similar expressions are used for the other time derivatives.

Numerical results

In most of the subsequent results, the value of the compressibility number B is 0.01. This is considerably larger than typical experimental values of B, which are of the order of $B = 0.0003$. Nevertheless, our objective, at this stage, is not to make comparisons with experiments but to qualitatively explore the proposed mechanism of instability. As already mentioned, a complete picture of the role of compressibility cannot be realized without including the reservoir (barrel) volume in the simulations. Moreover, we know from previous work on compressible Newtonian flow with slip along the wall (Georgiou and Crochet, 1994a, b) that the frequency of the oscillations becomes higher and the amplitude and the wavelength of the free surface waves decrease, as compressibility increases. Therefore, at smaller values of B, finer meshes and smaller time steps should be employed, in order to accurately compute the oscillating solution, and, consequently, the computational cost would be higher. The length of the die, ΔL, is also an important variable in compressible flow with slip along the wall, since it defines the amount of fluid that is being compressed and decompressed during one pressure-drop oscillation. As ΔL increases, the period and the amplitude of the pressure-drop and mass-flow-rate oscillations become larger (Georgiou and Crochet, 1994a). Studying the effect of ΔL is not of interest in the present work. We consider only the case of $\Delta L = 5$, i.e., we take the inflow plane at 5 radii upstream from the exit. The pressure drop ΔP is taken as the value of the pressure at the intersection of the inflow plane and the wall. The dimensionless slip numbers are the same as those used in Georgiou and Crochet (1994a, b): $A_1 = 1$, $A_2 = 20$ and $A_3 = 100$. We will first present results for the Poiseuille flow, i.e., when the extrudate region is excluded. The flow curves for $B = 0.01$ and Re = 0.01 and 1 are shown in Fig. 2. Due to the particular choice of A_2, both flow curves exhibit a maximum and a minimum. In all subsequent results,

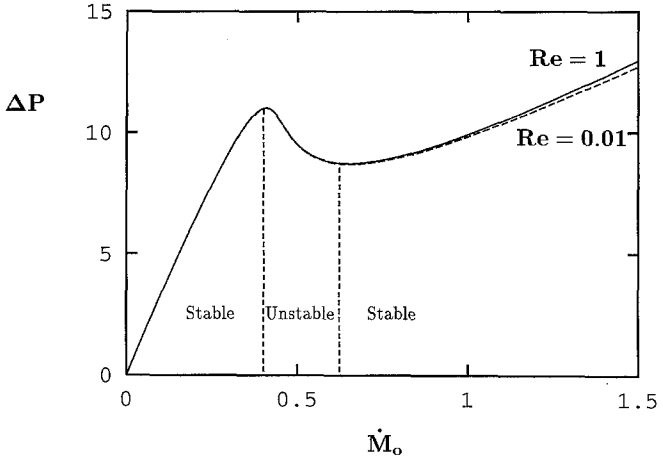

Fig. 2 Flow curves of compressible Poiseuille flow with slip at the wall for Re = 0.01 and 1; $B = 0.01$, $\Delta L = 5$

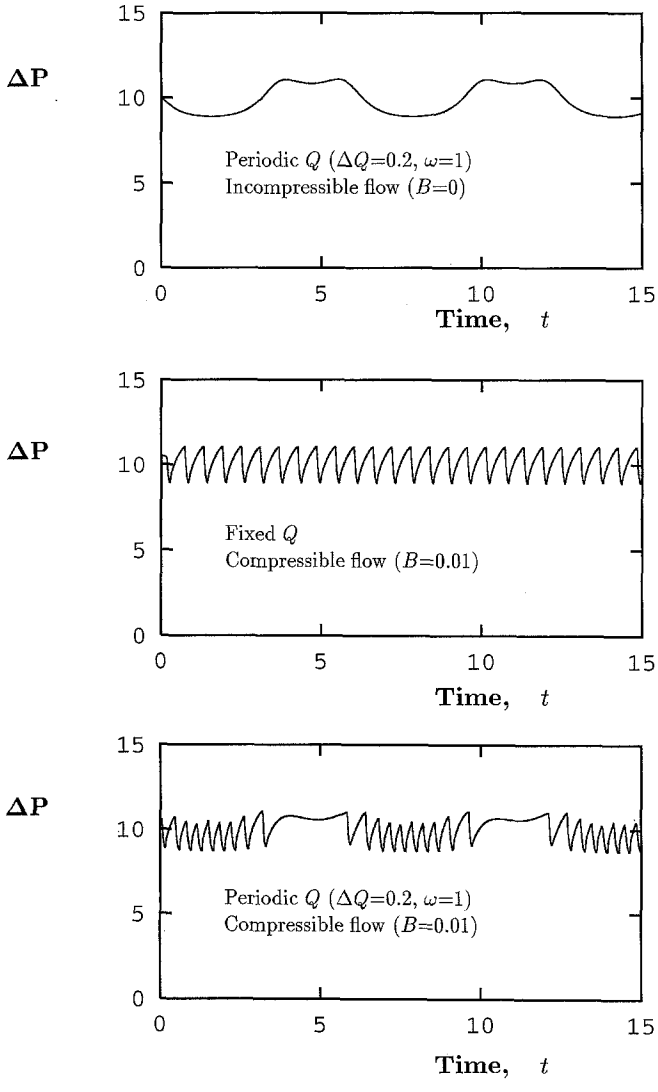

Fig. 3 Calculated pressure drops for Poiseuille flow; Re = 0.01, $Q_0 = 0.4071$, and $\Delta L = 5$

Rheologica Acta, Vol. 35, No. 6 (1996)

$Q_0 = 0.4071$, a value that corresponds to the negative-slope (i.e., unstable) part of the flow curves.

In Fig. 3, we compare the pressure drops obtained for Re = 0.01 in the following cases: i) incompressible flow ($B = 0$) with periodic volumetric flow rate at the inlet ($\Delta Q = 0.2$ and $\omega = 1$); ii) compressible flow ($B = 0.01$) with fixed volumetric flow rate at the inlet (Q_0 is actually perturbed by 0.1% at $t = 0$); iii) compressible flow ($B = 0.01$) with periodic volumetric flow rate at the inlet ($\Delta Q = 0.2$ and $\omega = 1$). In case i), the oscillations are due to the periodicity of the volumetric flow rate at the inlet; in case ii), they are due to the combination of compressibility and nonlinear slip and they are self-sustained. Finally, in case iii), the oscillations are the result of the synergy of the above two mechanisms. In Fig. 3c, we observe that the pressure drop is characterized by alternating oscillatory and relatively smooth regimes for this particular choice of ω. (The frequency of the self-sustained oscillations of case ii) is much higher than that of the imposed volumetric flow rate.) This pattern is followed by the mass flow rate at the outlet as well. This is shown in Fig. 4, where we plotted the calculated mass flow rates at the inlet and the outlet.

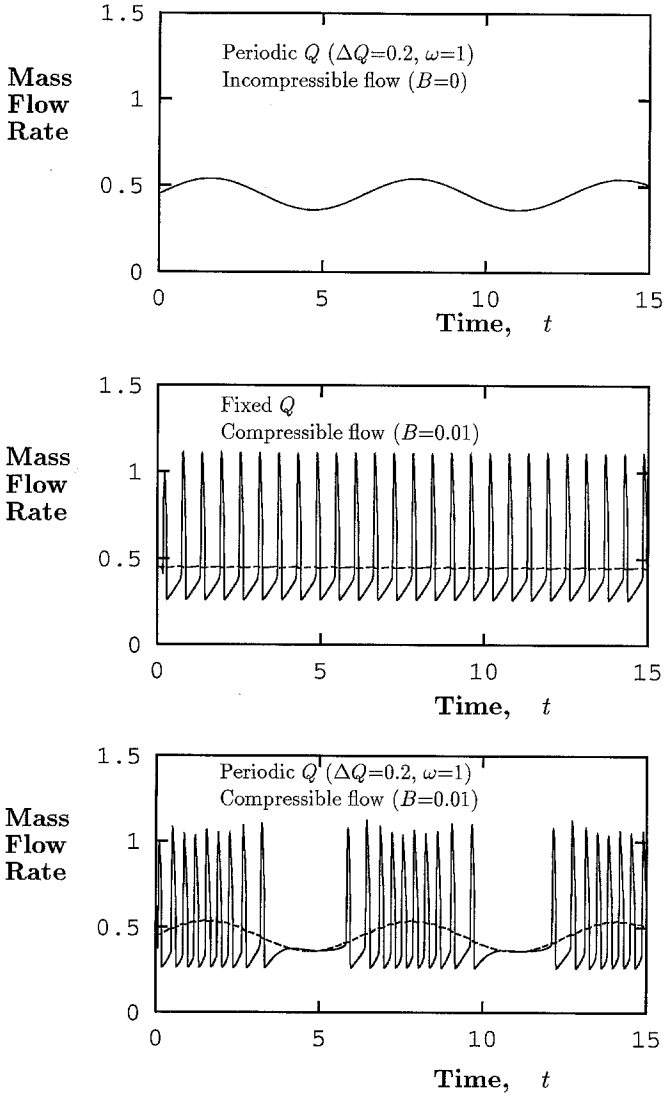

Fig. 4 Calculated mass flow rates at the inlet (– – –) and the outlet (———) for Poiseuille flow; Re = 0.01, $Q_0 = 0.4071$, and $\Delta L = 5$

The effect of ω on the mass flow rate oscillation patterns is illustrated in Fig. 5 (Re = 0.01) and 6 (Re = 1). We observe that completely different patterns may be obtained depending on the values of Re, ΔQ, and ω.

We now proceed to the solution of the extrudate swell problem, i.e., we include the extrudate region in our calculations. As expected, different patterns of free surface oscillations arise, depending on the type of the oscillations generated in the die. One difficulty in the case of the extrudate swell problem is that the finite element mesh in the extrudate region should be sufficiently refined and long in order to accurately capture the free surface oscillations. In all subsequent results, the length of the extrudate is taken to be five radii.

In Figs. 7–9, we show the mass flow rates, the pressure drop, and the free surface profile corresponding to a pressure drop maximum (after periodicity is established) for the same cases as those of Fig. 3: i) incompressible flow ($B = 0$) with periodic volumetric flow rate at the inlet ($\Delta Q = 0.2$ and $\omega = 1$); ii) compressible flow ($B = 0.01$) with fixed volumetric flow rate at the inlet; iii) Compressible flow ($B = 0.01$) with periodic volumetric flow rate at the inlet ($\Delta Q = 0.2$ and $\omega = 1$). In the last case, the combination of compressibility, nonlinear slip at the wall and periodicity at the inlet leads to oscillatory patterns characterized by alternating smooth and oscillatory regimes. As shown in Fig. 9c, the free surface oscillations follow the same pattern, which is similar to that observed experimentally with the stick-slip instability (Kalika and Denn, 1987). The alternating smooth and rough regions move downstream following the flow, as illustrated in Fig. 10, where we plot various free surface profiles obtained during a single cycle of the pressure drop oscillations.

Similar calculations have been carried out for other values of Re and ΔQ. In Figs. 11–13, we show results obtained for Re = 1. In Fig. 11, we plot the mass flow rates, the pressure drop and the free surface profile corresponding to a pressure drop maximum obtained for incompressible flow ($B = 0$) with periodic volumetric flow rate at the inlet ($\Delta Q = 0.1$ and $\omega = 2.5$). In Fig. 12, we plot the results obtained for compressible flow ($B = 0.01$) with fixed volumetric flow rate at the inlet ($\Delta Q = 0$). The periods of the oscillations in the above two cases are essentially the same. Finally, in Fig. 13, we show the results obtained when compressibility ($B = 0.01$) and periodicity at the inlet ($\Delta Q = 0.1$ and $\omega = 2.5$) are combined. It is interesting to note that, in this particular case,

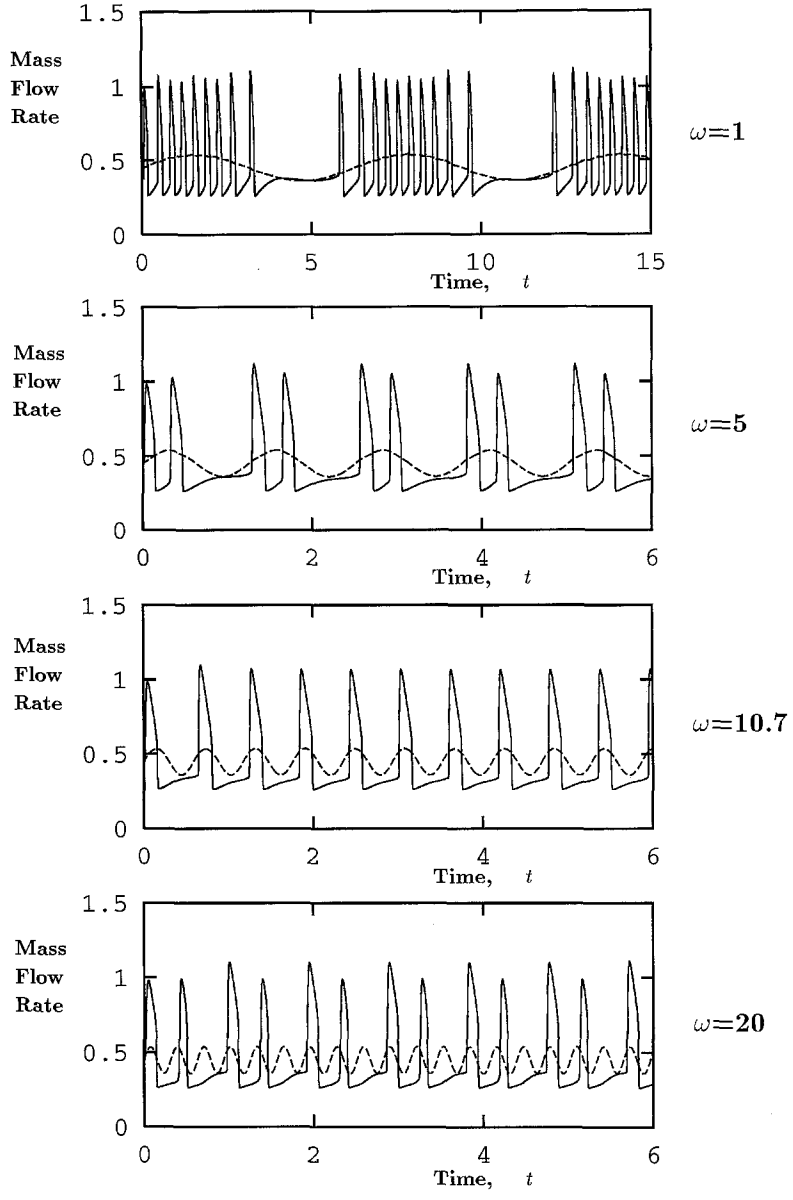

Fig. 5 Calculated mass flow rates at the inlet (– – –) and the outlet (———) for compressible Poiseuille flow; Re = 0.01, $B = 0.01$ and $\Delta Q = 0.2$

Rheologica Acta, Vol. 35, No. 6 (1996)

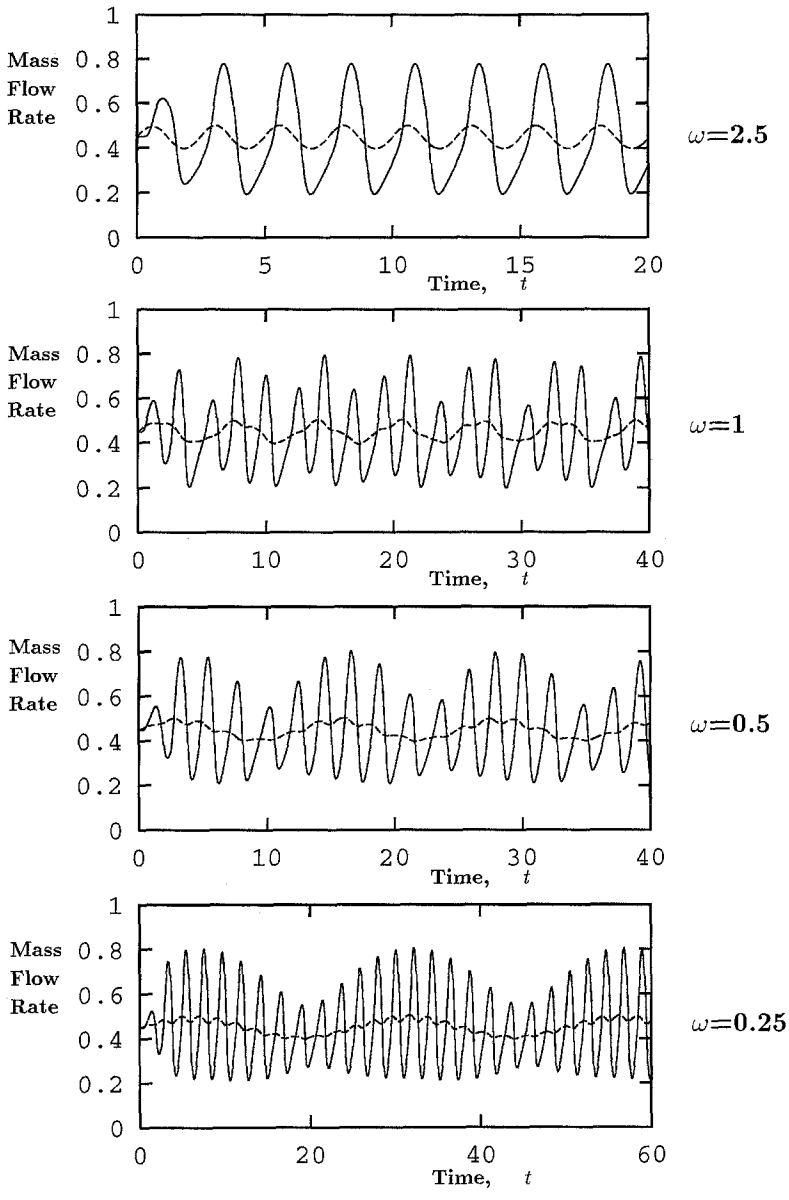

Fig. 6 Calculated mass flow rates at the inlet (– – –) and the outlet (———) for compressible Poiseuille flow; Re = 1, $B = 0.01$ and $\Delta Q = 0.1$

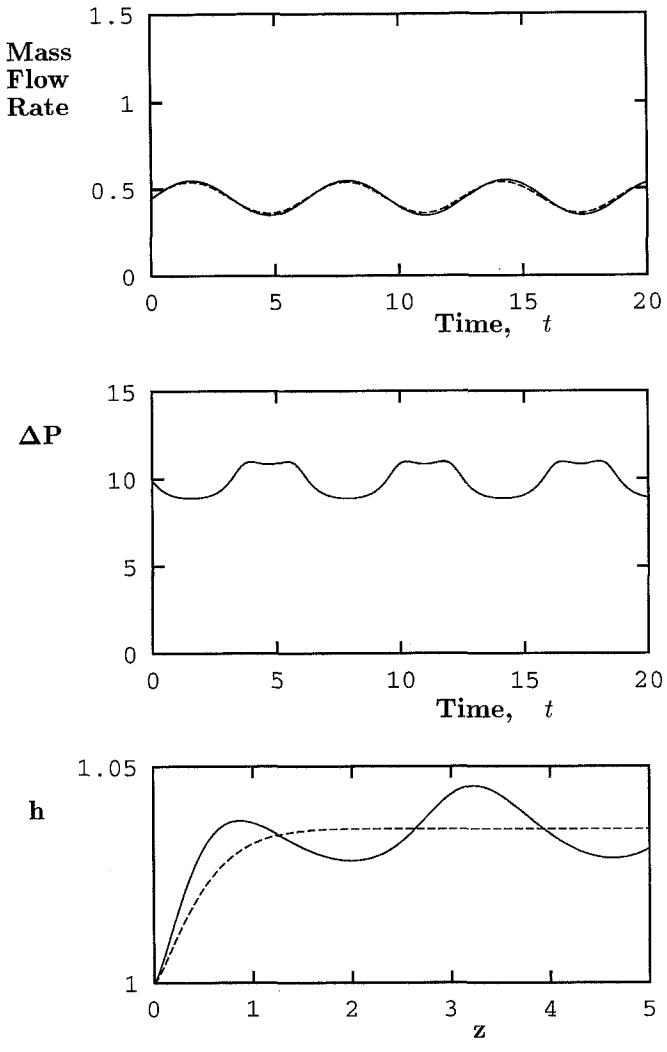

Fig. 7 Results for incompressible extrudate-swell flow with periodic Q, Re = 0.01, $\Delta Q = 0.2$, and $\omega = 1$: **A** Mass flow rates at the inlet (– – –) and outlet (———); **B** pressure drop; **C** free surface profile at a pressure drop maximum (the broken curve is the steady-state solution)

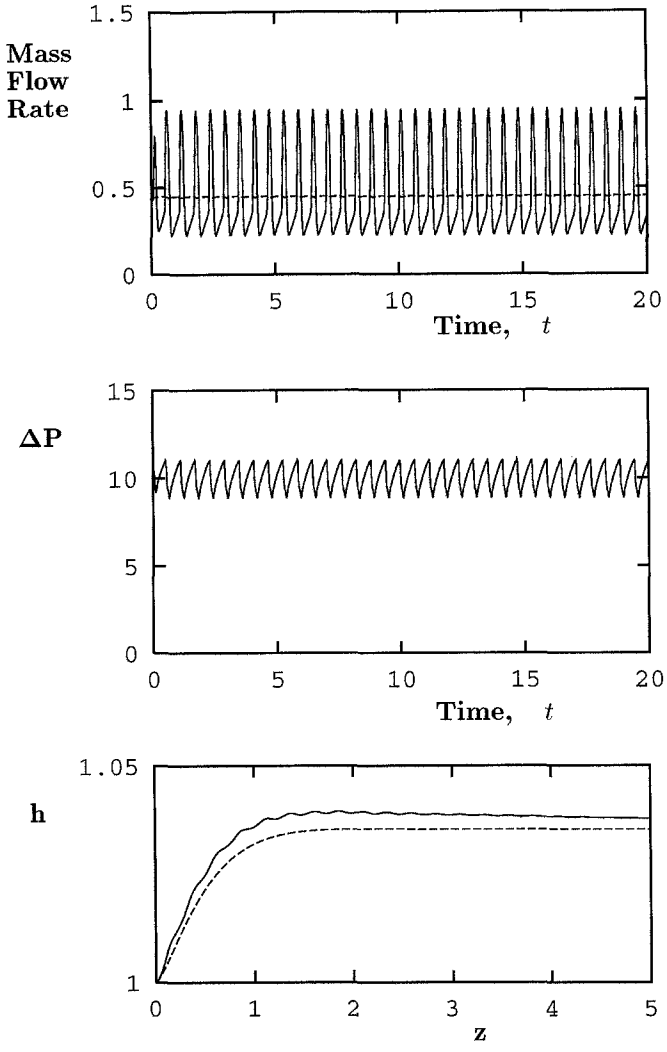

Fig. 8 Results for compressible extrudate-swell flow with fixed Q, Re = 0.01, $B = 0.01$: **A** Mass flow rates at the inlet (– – –) and outlet (———); **B** pressure drop; **C** free surface profile at a pressure drop maximum (the broken curve is the steady-state solution)

the pattern of the free surface oscillations appears to be similar to those of the former two cases, but the amplitude of the generated waves is considerably amplified (it is much greater than the sum of the amplitudes in the former two cases).

In Figs. 14 and 15, we show results obtained with Re = 1 and a lower compressibility number, $B = 0.001$. In Fig. 14, the volumetric flow rate at the inlet is constant. The oscillations are caused by the combination of nonlinear slip and compressibility. By comparing these results to their counterparts for $B = 0.01$ (Fig. 12), we observe that the amplitude and the wavelength of the free-surface waves decrease with B (see also Ref. [9]). If, however, the volumetric flow rate at the inlet is periodic, as in Fig. 15 where we show results with $\Delta Q = 0.1$ and $\omega = 2.5$, the pattern of the free surface waves is altered and the free surface waves become less regular (Fig. 15c).

We close this section by pointing out that, despite the fact that the proposed mechanism of extrusion instability leads to extrudates which resemble to actual extrudates, a number of important factors and experimental variables should be taken into account before attempting comparisons with experimental observations. First of all, an appropriate constitutive equation and a more realistic slip equation, such as those of El Kissi and Piau (1989), Leonov (1990) and Hatzikiriakos and Dealy (1992b),

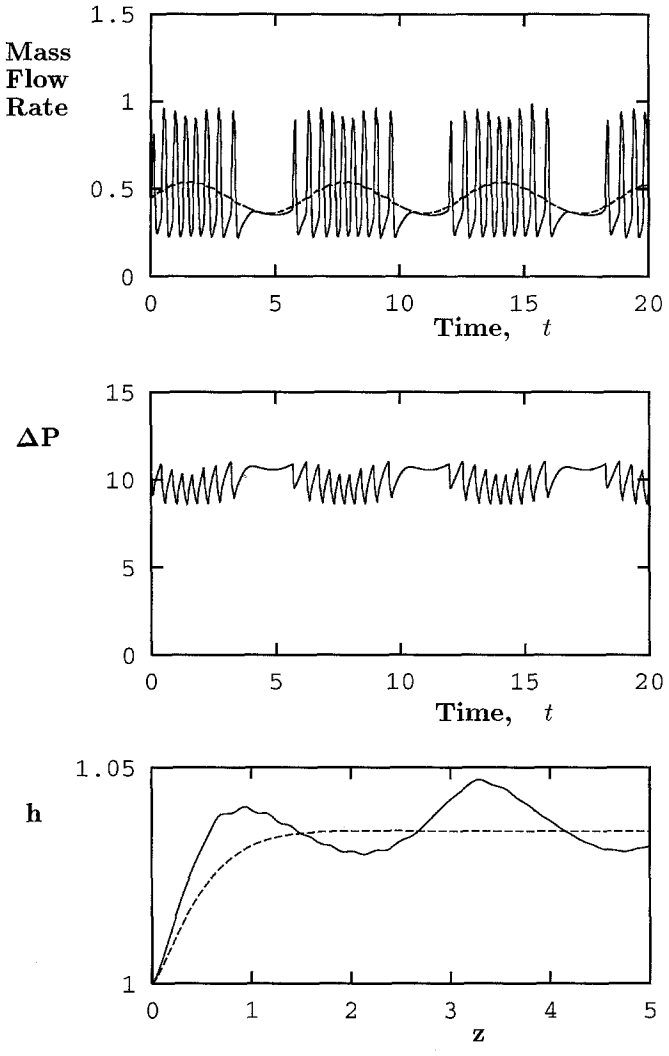

Fig. 9 Results for compressible extrudate-swell flow with periodic Q, Re = 0.01, B = 0.01, ΔQ = 0.2, and ω = 1: **A** Mass flow rates at the inlet (– – –) and outlet (———); **B** pressure drop; **C** free surface profile at a pressure drop maximum (the broken curve is the steady-state solution)

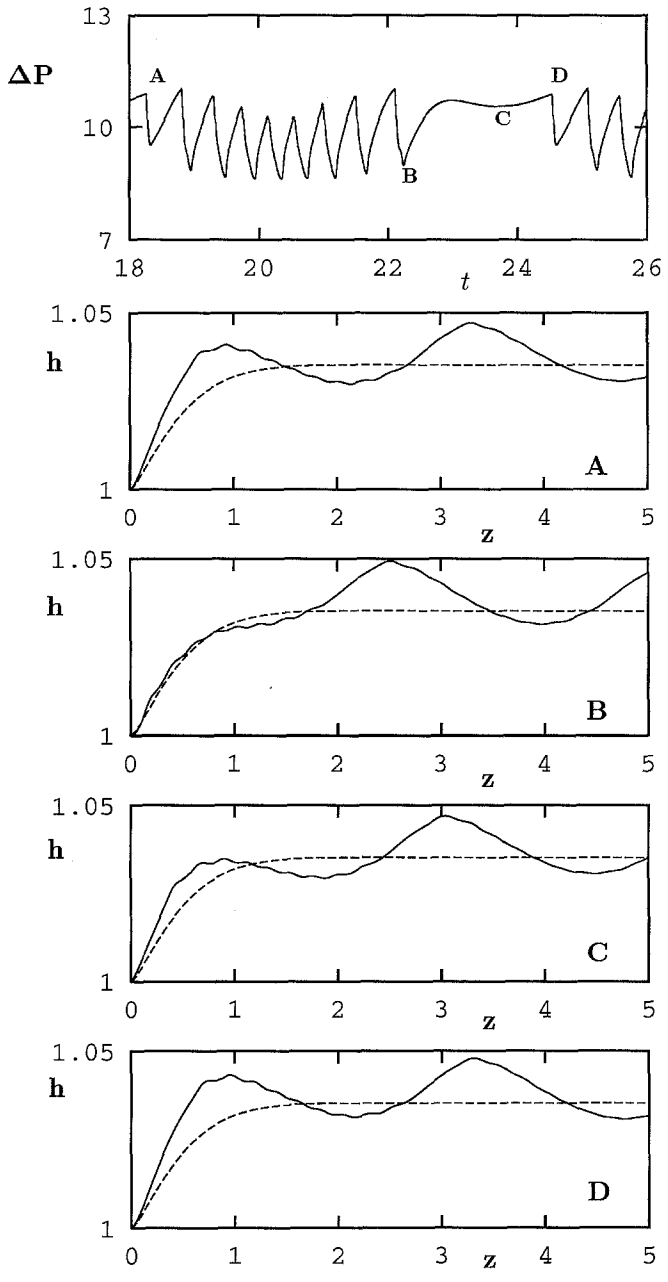

Fig. 10 Free surface profiles of compressible extrudate-swell flow with periodic Q during one cycle; Re = 0.01, B = 0.01, ΔQ = 0.2 and ω = 1

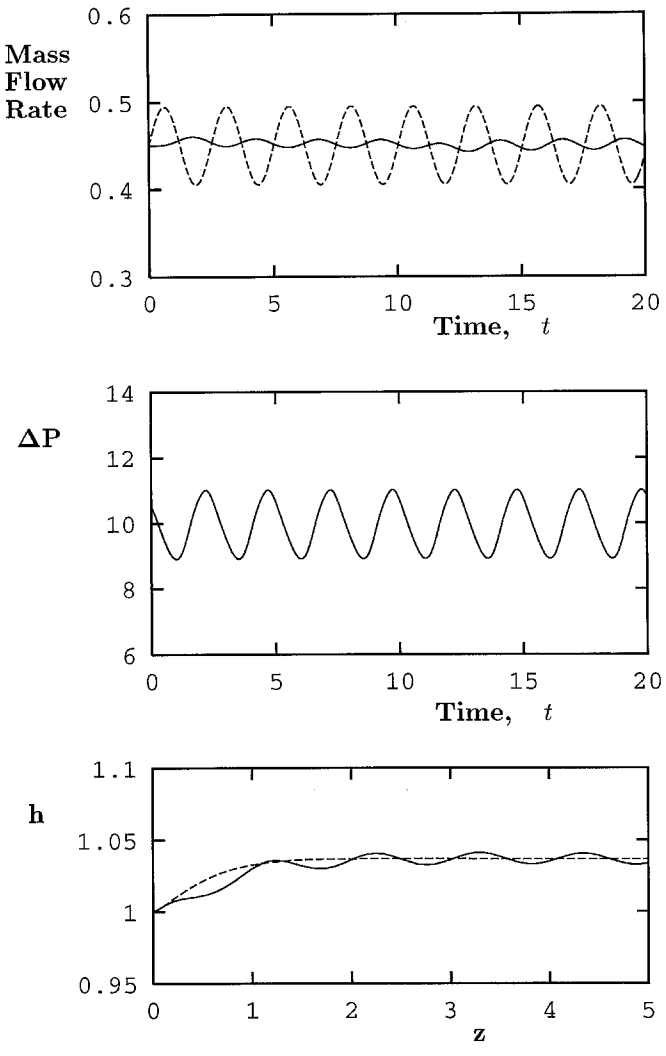

Fig. 11 Results for incompressible extrudate-swell flow with periodic Q, Re = 1, $\Delta Q = 0.1$ and $\omega = 2.5$: **A** Mass flow rates at the inlet (– – –) and outlet (———); **B** pressure drop; **C** free surface profile at a pressure drop maximum (the broken curve is the steady-state solution)

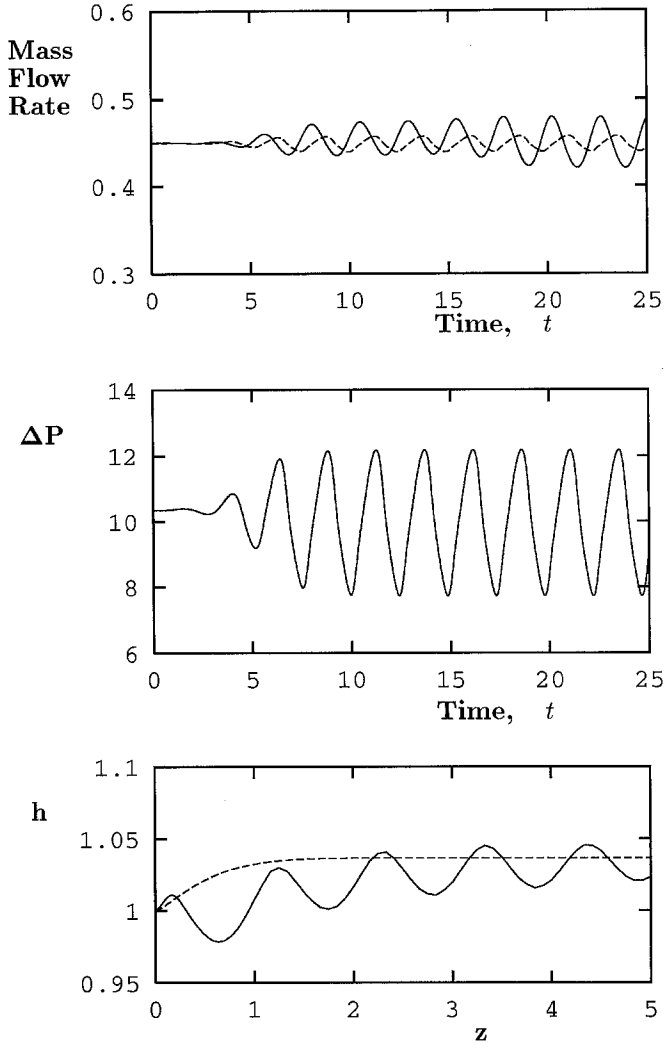

Fig. 12 Results for compressible extrudate-swell flow with fixed Q, Re = 1 and $B = 0.01$: **A** Mass flow rates at the inlet (– – –) and outlet (———); **B** pressure drop; **C** free surface profile at a pressure drop maximum (the broken curve is the steady-state solution)

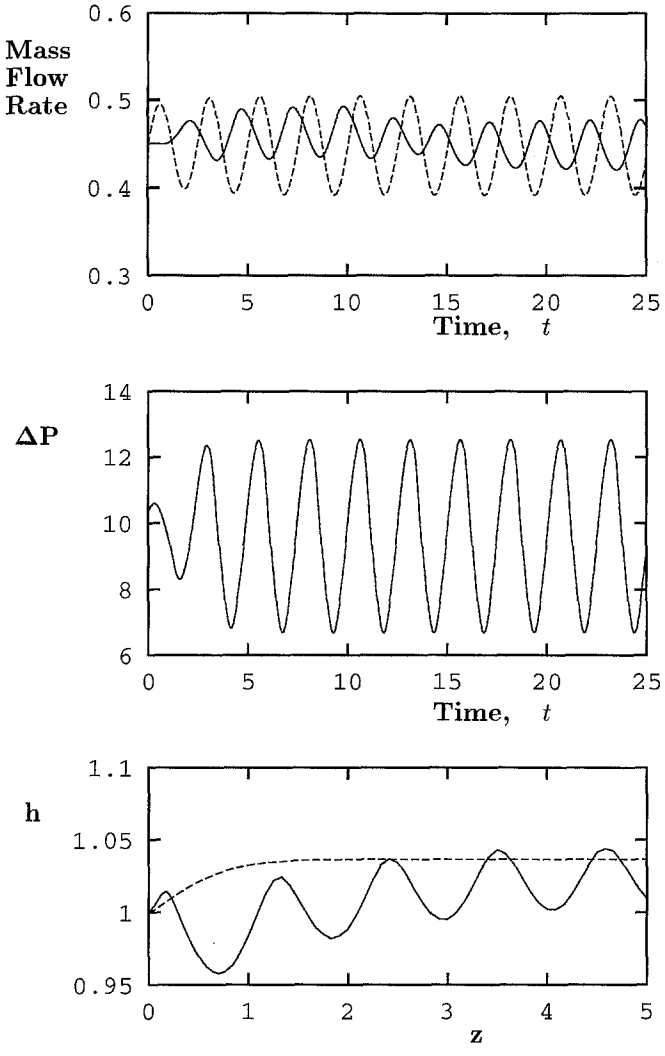

Fig. 13 Results for compressible extrudate-swell flow with periodic Q, Re = 1, $B = 0.01$, $\Delta Q = 0.1$ and $\omega = 2.5$: **A** Mass flow rates at the inlet (– – –) and outlet (———); **B** pressure drop; **C** free surface profile at a pressure drop maximum (the broken curve is the steady-state solution)

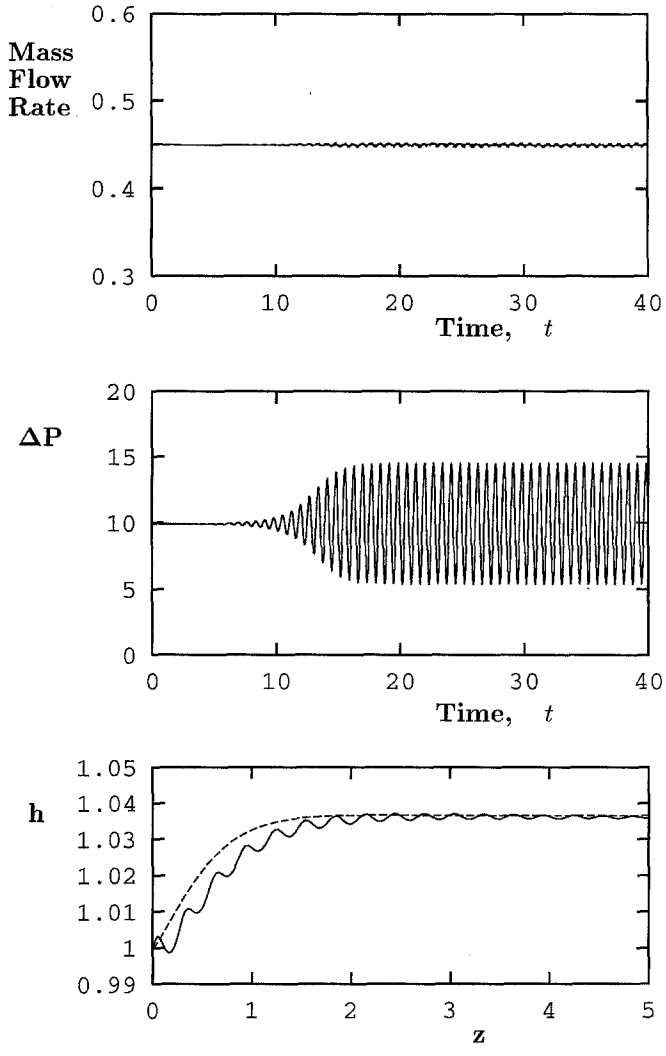

Fig. 14 Results for compressible extrudate-swell flow with fixed Q, Re = 1, and $B = 0.001$: **A** Mass flow rates at the inlet (– – –) and outlet (———); **B** pressure drop; **C** free surface profile at a pressure drop maximum (the broken curve is the steady-state solution)

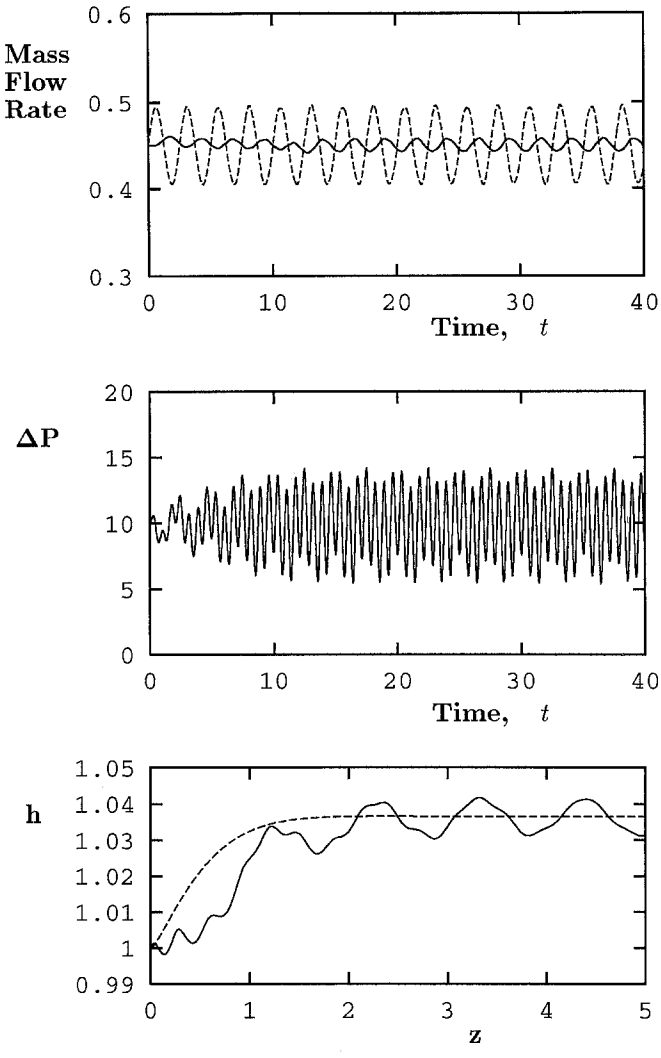

Fig. 15 Results for compressible extrudate-swell flow with periodic Q, Re = 1, $B = 0.001$, $\Delta Q = 0.1$ and $\omega = 2.5$: **A** Mass flow rates at the inlet (– – –) and outlet (———); **B** pressure drop; **C** free surface profile at a pressure drop maximum (the broken curve is the steady-state solution)

should be used. This might lead to considerably different oscillatory flow patterns, since the size and the shape of the pressure and mass-flow-rate oscillations are dictated by the shape of the flow curve. Note that the unstable regime of the slip equation used in the present work is rather narrow. Experimental slip data are always given in a log-log plot and the unstable regime is up to five times broader than the left stable regime. Finally, we underline the fact that continuum modeling obviously cannot capture phenomena related to molecular dynamics, such as polymer segregation, micro-slip and cracking, on which some recently suggested explanations for the small-amplitude high-frequency distortions of the extrudate (i.e. for sharkskin) are based (Chen and Joseph, 1992; Tremblay, 1991; El Kissi and Piau, 1994).

Conclusion

We have presented a mechanism of extrusion instability which is based on the combination of nonlinear slip and compressibility and the assumption of periodic volumetric flow rate at the inlet of the die. We assume that slip occurs along the wall of the die following an arbitrary nonlinear slip model that relates the shear stress to the velocity at the wall and is of negative slope in some critical range of the slip velocity. Steady-state solutions in the negative-slope regime of the slip equation are linearly unstable. Compressibility, introduced by means of a simple linear equation of state, gives rise to the alternate storage and release of elastic energy which generate self-sustained oscillations of the pressure and the mass flow rate at the exit. The assumption of periodic volumetric flow rate at the inlet accounts for possible upstream instabilities and results in more involved oscillatory flow patterns. For certain ranges of the relevant parameters, we have obtained extrudate surfaces with alternating oscillatory and relatively smooth regions, similar to those observed with the stick-slip instability.

Acknowledgments The author is grateful to Prof. Marcel Crochet of Unité de Mécanique Appliquée, Université Catholique de Louvain, for his support, hospitality, and helpful discussions. This paper presents research results of the Belgian Programme on Interuniversity Poles of Attraction, initiated by the Belgian State, Prime Minister's Office for Science, Technology and Culture. The scientific responsibility rests with the author.

References

Brasseur E, Georgiou GC, Crochet MJ (1966) The time-dependent extrudate-swell problem of an Oldroyd-B fluid with slip along the wall. Symposium on Rheology and Computational Fluid Mechanics, Nicosia (Cyprus), July 4–5

Chen K, Joseph DD (1992) Elastic short wave instability in extrusion flows of viscoelastic liquids. J Non-Newt Fluid Mech 42:189–211

Denn MM (1990) Issues in viscoelastic fluid mechanics. Annu Rev Fluid Mech 22: 13–34

Denn MM (1992) Surface-induced effects in polymer melt flow. In: Moldenaers P, Keunings R (eds) Theoretical and Applied Rheology. Elsevier Science Publishers: 45–49

El Kissi N, Piau JM (1989) Ecoulement de fluides polymères enchevêtrés dans un capillaire. Modélisation du glissement macroscopique à la paroi. C R Acad Sci Paris t 309, Série II:7–9

El Kissi N, Piau JM (1994) Adhesion of linear low density polyethylene for flow regimes with sharkskin. J Rheol 38(5): 1447–1463

Georgiou GC, Papanastasiou TC, Wilkes JO (1988) Laminar jets at high Reynolds and high surface tension. AIChE J 24, No. 9:1559–1562

Georgiou GC, Crochet MJ (1994a) Compressible viscous flow in slits, with slip at the wall. J Rheology 38:639–654

Georgiou GC, Crochet MJ (1994b) Time-dependent compressible extrudate-swell problem with slip at the wall. J Rheology 38:1745–1755

Georgiou GC (1996) On the stability of the shear flow of a viscoelastic fluid with slip along the fixed wall. Rheol Acta 35:39–47

Hatzikiriakos SG, Dealy JM (1992a) Wall slip of molten high density polyethylenes. II. Capillary Rheometer studies. J Rheol 36:703–741

Hatzikiriakos SG, Dealy JM (1992b) Role of slip and fracture in the oscillating flow of HDPE in a capillary. J Rheol 36: 845–884

Hill DA, Hasegawa T, Denn MM (1990) On the apparent relation between adhesive failure and melt fracture. J Rheology 34:891–918

Kalika DS, Denn MM (1987) Wall slip and extrudate distortion in linear low-density polyethylene. J Rheol 31:815–834

Kolkka RW, Malkus DS, Hansen MG, Ierley GR, Worthing RA (1988) Spurt phenomena of the Johnson-Segalman fluid and related models. J Non-Newtonian Fluid Mech 29:303–335

Larson RG (1992) Instabilities in viscoelastic flows. Rheol Acta 31:213–263

Leonov AI (1990) On the dependence of friction force on sliding velocity in the theory of adhesive friction of elastomers. Wear 141:137–145

Moynihan RH, Baird DG, Ramanathan R (1990) Additional observations on the surface melt fracture behavior of linear low-density polyethylene. J Non-Newt Fluid Mech 36:255–263

Pearson JRA, Petrie CJS (1965) On the melt-flow instability of extruded polymers. Proc 4th Int Rheological Congress 3:265–282

Pearson JRA (1985) Mechanics of Polymer Processing. Elsevier, London

Piau JM, El Kissi N, Tremblay B (1990) Influence of upstream instabilities and wall slip on melt fracture and sharkskin phenomena during silicones extrusion through orifice dies. J Non-Newtonian Fluid Mech 34:145–180

Piau JM, El Kissi N (1992) The influence of interface and volume properties of polymer melts on their die flow stability. In: Moldenaers P, Keunings R (eds) Theoretical and Applied Rheology. Elsevier Science Publishers: 70–74

Piau JM, El Kissi N, Toussaint F, Mezghani A (1995) Distortions of polymer melt extrudate and their elimination using slippery surfaces. Rheol Acta 34:40–57

Tremblay B (1991) Sharkskin defects of polymer melts: The role of cohesion and adhesion. J Rheol 35:985–998